Chapter 4

Microstructural Evolution and Formation Mechanism of the Interface between Titanium and Zirconia Annealed at 1550°C

4.1 Introduction

Extensive studies have been carried out on the interface reaction between titanium and zirconia in the last few decades.[1-3] Weber *et al.*[1] indicated that zirconia was blackened by a limited solid solution of titanium in zirconia, when the titanium melt reacted with the ZrO_2 crucible. In discussing the effect of the Ti additive on the microstructure of zirconia at 2000°C/3 h, Ruh *et al.*[2] found that the liquid titanium diffused into zirconia to form various reaction layers. Zhu *et al.*[3] investigated the wettability and the interaction between pure liquid titanium and yttria-stabilized zirconia by sessile drop method in Ar atmosphere at 1700°C. They found that there existed two distinct chemical reaction layers in the interface. Recently, Lin and his coworkers[4-6] have been undergoing an intense investigation on the diffusional reaction between titanium and zirconia. Using TEM/EDS analyses, Lin and Lin[4] indicated that an ordered titanium suboxide (Ti_3O) and the orthorhombic lamellae Ti_2ZrO were formed in the solid solution of α-Ti(O) during cooling from 1700°C. In addition to the lamellar Ti_2ZrO and α-Ti(O), Lin and Lin[5] observed the orthorhombic β'-Ti(Zr, O) and an spherical ordered Ti_2ZrO phase in the metal side after annealing at 1550°C. By focusing upon the zirconia side far away from the original interface of Ti and ZrO_2, Lin and Lin[6] also observed twinned *t'*-ZrO_{2-x}, lenticular *t*-ZrO_{2-x}, ordered *c*-ZrO_{2-x}, and the intergranular α-Zr after the Ti/ZrO_2 diffusion couple was annealed at 1550°C using analytical TEM.

In order to shed light on the microstructural evolution of the various distinct reaction layers between titanium and zirconia, the Ti/ZrO_2 diffusion couple was isothermally annealed in argon at 1550°C for various periods in the present study, and the microstructures were characterized using analytical scanning electron microscopy (SEM), analytical transmission electron microscopy (TEM), and an electron probe microanalyzer (EPMA). Finally, the formation mechanisms, as well as microstructural evolution, of the reaction layers between titanium and zirconia were proposed.

4.2 Experimental Procedures

Bulk ZrO_2 specimens used in this study were prepared from the powder of 3 mol% Y_2O_3 partially stabilized zirconia (with a nominal composition of > 94 wt% ZrO_2 + HfO_2 (HfO_2 accounts for approximately 2~3% of this total), 5.4 wt% Y_2O_3, < 0.001 wt% Fe_2O_3, < 0.01 wt% SiO_2, < 0.005 wt% Na_2O, < 0.005 wt% TiO_2, < 0.02 wt% Cl, < 0.005 wt% SO_4^{2-}; Toyo Soda Mfg. Co., Tokyo, Japan) by hot-pressing (Model HP50-MTG-7010, Thermal Techno. Inc., Santa Rosa, CA). The bulk ZrO_2 and commercially available titanium billets (with a nominal composition of 99.31 wt% Ti, 0.25 wt% O, 0.01 wt% H, 0.03 wt% N, 0.10 wt% C, 0.30 wt% Fe; Kobe Steel, Ltd., Tokyo, Japan) were cut and machined to 14 mm x 14 mm x 5 mm in dimensions. The sandwiched samples, one Ti in between two ZrO_2 specimens, were slightly pressed and annealed at 1550°C for 0.5, 3, and 6 hours in an atmosphere of Ar. The hot-pressing procedures of bulk ZrO_2 and the sandwiched samples have been described in detail elsewhere.[5]

The cross-sectional SEM, TEM and EPMA specimens perpendicular to the interface of titanium and zirconia were cut, ground, and polished by standard

procedures. The microstructures at the interface were observed using an analytical SEM (Model JSM 6500F, JEOL Ltd., Tokyo, Japan) and an analytical TEM (Model JEM 2000Fx, JEOL Ltd., Tokyo, Japan). The quantitative composition analyses were carried out based on the principle of the Cliff-Lorimer standardless technique[7] by an EDS (Mode ISIS300, Oxford Instrument Inc., London, UK) attached to the TEM. The backscattered electron images (BEI) had been taken on the SEM. The compositions of those phases in the reaction layers at the interface between Ti and ZrO_2 were quantitatively measured by an EPMA (JXA-8800M, JEOL, Tokyo, Japan) with the aid of an atomic number, absorption, and fluorescence corrections (ZAF) program.[8] The measurement conditions for EPMA were as follows: the accelerating voltage was 15 KV; the probe current was 1.5 x 10^{-8}A; the beam diameters was 1 μm.

4.3 Results and Discussion

4.3.1 Formation Mechanism of Various Reaction Layers

Figures 4.1(a), (b), and (c) display the backscattered electron images of the cross-section normal to the interface between Ti and ZrO_2 after reaction at 1550°C for 0.5, 3, and 6 h, respectively. Titanium was in the left-hand side, while zirconia was in the other side. The arrows in the upper middle of these figures indicated the original interface of Ti and ZrO_2. There were five reaction layers, designed as "A," "B," "C," "D," and "E," in the metal side, while only two distinct reaction layers, designed as "F" and "G," were found in the zirconia side. The thickness of the individual reaction layers increased with the annealing time. Moreover, in the reaction layer "G," zirconia grains grew obviously and α-Zr (brighter) was coarsened and became isolated after annealing at 1550°C for 6 h [Fig. 4.1(c)]. The existence of the pores in the ceramic side was attributed to the Kirkendall effect, since zirconium and oxygen diffused to the titanium side much faster

than titanium diffused toward the zirconia side.

Figure 4.2(a) displays the backscattered electron image of the cross-section normal to the interface between Ti and ZrO_2 after reaction at 1550°C/6 h. The distributions of Y, Ti, Zr, and O elements in the interface were demonstrated by x-ray mappings in Fig. 4.2(b)-(e), respectively. The original interface (the arrows) was deliberately located according to the results of the characteristic K_α x-ray map of yttrium [Fig. 4.2(b)], which was relatively immobile compared with elements Zr, O, and Ti. Because Ti and Zr are isomorphous elements and the difference in their atomic radii are very small,[9] they are readily substituted for each other. Figures 2(c) and (d) confirmed that the interdiffusion of Ti and Zr was intense and the diffusion distance of Ti and Zr was nearly equal. Figure 4.2(e) shows that oxygen showed a long-range diffusion into titanium, causing the formation of the oxygen-containing α-Ti.

Figure 4.3 displays the backscattered electron image of the reaction layers "A," "B," and "C" between Ti and ZrO_2 after reaction at 1550°C/6 h. The reaction layer "A" was α-Ti which dissolved a large amount of oxygen and a little zirconium. The quantitative analyses by the EPMA show that it contained 71.30 at.% Ti, 0.97 at.% Zr, and 27.72 at.% O corresponding to be α-Ti(O). The formation of α-Ti(O) was caused by the oxidation-reduction reaction of titanium and zirconia and could be expressed as following reactions:

$$ZrO_2 + Ti \xrightarrow{\text{heating}} ZrO_{2-x} + \beta\text{-}Ti(O) \quad (1)$$

$$\beta\text{-}Ti(O) \xrightarrow{\text{cooling}} \alpha\text{-}Ti(O) \quad (2)$$

The reaction layer "B" with a continuous lamellar morphology consisted of α-Ti (gray) and needle-like Ti_2ZrO (bright). The thin continuous layer, consisting of lamellar α-Ti and Ti_2ZrO, were first found in the present study. Unlike these continuous lamellar phases found in the present study, Lin and Lin[5] reported that the Ti_2ZrO lamellae were precipitated from plate-like α-Ti (O, Zr) by eutectoid reaction during cooling. The formation of lamellar α-Ti (O) and Ti_2ZrO in the thin continuous layer (the reaction layer "B") was expressed as following reactions:

$$ZrO_2 + Ti \xrightarrow{\text{heating}} ZrO_{2-x} + \beta\text{-}Ti(Zr, O) \quad (3)$$

$$\beta\text{-}Ti(Zr, O) \xrightarrow{\text{cooling}} \alpha\text{-}Ti(Zr, O) \xrightarrow{\text{cooling}} \alpha\text{-}Ti(Zr, O) + Ti_2ZrO \quad (4)$$

The reaction layer "C" consisted of β'-Ti (bright) and the lamellae of Ti_2ZrO and α-Ti (gray). At high temperatures, the primary α-Ti dissolved a large amount of zirconium and oxygen, forming metastably α-Ti(Zr, O), and thus resulted in the precipitation of the lamellae Ti_2ZrO during cooling. Meanwhile, the β-Ti, which dissolved a large of Zr and O, transformed to orthorhombic β'-Ti(Zr, O) solid solution during cooling. The coexistence of α-Ti (O), Ti_2ZrO, and β'-Ti (O, Zr) can be expressed as following reactions:

$$ZrO_2 + Ti \xrightarrow{\text{heating}} ZrO_{2-x} + \alpha\text{-}Ti(Zr, O) + \beta\text{-}Ti(Zr, O) \quad (5)$$

$$\alpha\text{-}Ti(Zr, O) + \beta\text{-}Ti(Zr, O) \xrightarrow{\text{cooling}} \alpha\text{-}Ti(Zr, O) + Ti_2ZrO + \beta'\text{-}Ti(Zr, O) \quad (6)$$

Figure 4.4 displays the backscattered electron image of the reaction layer "D" in the interface between Ti and ZrO_2 after reaction at 1550°C/6 h. The original interface of titanium and zirconia was beyond the right-hand side of the micrograph. When the concentration of zirconia is small like the region in the left-hand side of Figure 4.4, the reaction layer "D" would consist of the acicular α-Ti (dark) in the β-Ti matrix (gray). The precipitation of the acicular α-Ti(O, Zr) was expressed by the following reactions:

$$ZrO_2 + Ti \xrightarrow{\text{heating}} ZrO_{2-x} + \beta\text{-}Ti(Zr, O) \quad (3)$$

$$\beta\text{-}Ti(Zr, O) \xrightarrow{\text{cooling}} \alpha\text{-}Ti(Zr, O) + \beta'\text{-}Ti(Zr, O) \quad (7)$$

Since the zirconium was the stabilizer of β-Ti, fewer acicular α-Ti was observed in the right side of Fig. 4.4, where a higher concentration of Zr existed in titanium. Also shown in Fig. 4.4, the amount of the acicular α-Ti increased with the distance away from interface. The reaction layer "D," which dissolved a significant amount of zirconium (beta-stabilizer) and oxygen (alpha-stabilizer), was composed of α + β titanium with Zr and O in solid solution. For comparison, it is worth noting that the acicular-like α-Ti were also found in α + β titanium alloys such as Ti-6Al-4V or Ti-8Al-1Mo-1alloys.[10]

The orientation relationship of the acicular α-Ti and the β'-Ti has been subjected to an intense investigation. Figure 4.5(a) shows the TEM micrograph (bright field image, BFI) of the cross-section normal to the interface of Ti and ZrO_2 after reaction at 1550°C/6 h. The acicular α-Ti and the β'-Ti were identified as hexagonal and orthorhombic crystal structures, respectively, from the superimposed selected area diffraction patterns

(SADPs) as shown in Fig. 4.5(b). The selected area diffraction patterns in Fig. 4.5(b) were schematically redrawn in Fig. 4.5(c) with the diffraction spots being indexed. The orientation relations between α-Ti and β'-Ti were thus identified as follows: $[2\bar{1}\bar{1}0]_{\alpha\text{-Ti}}$ // $[001]_{\beta'\text{-Ti}}$ and $(0001)_{\alpha\text{-Ti}}$ // $(100)_{\beta'\text{-Ti}}$. Moreover, the lattice constants of β'-Ti orthorhombic unit cell were calculated as follows: a_o = 0.58 nm, b_o = 0.84 nm and c_o = 0.61 nm, and those of α-Ti hexagonal unit cell are a_h= b_h= 0.30 nm, c_h= 0.46 nm. Figure 4.5(d) shows the EDS spectrum of the acicular α-Ti, revealing that it comprised 54.0 at.% Ti, 13.4 at.% Zr, and 32.8 at.% O. Figure 4.5(e) shows the EDS spectrum of the β'-Ti, consisting of 58.1 at.% Ti, 30.7 at.% Zr, and 11.2 at.% O. Since Zr is a stabilizer of β-titanium, it is not surprising that β'-Ti(Zr, O) contains much more Zr than α-Ti(Zr, O) does.

Figure 4.6(a) shows the TEM micrograph (bright field image, BFI) of the cross-section normal to the interface of Ti and ZrO_2 after reaction at 1550°C/6 h. Another orientation relationship of the acicular α-Ti and the β'-Ti was identified by the superimposed SADPs [Fig. 4.6(b)]. The SADPs were redrawn and indexed in Fig. 4.6(c). The orientation relations were recognized as follows: $[2\bar{1}\bar{1}0]_{\alpha\text{-Ti}}$ // $[021]_{\beta'\text{-Ti}}$ and $(0001)_{\alpha\text{-Ti}}$ // $(1\bar{1}2)_{\beta'\text{-Ti}}$. Figure 4.6(d) displays the image, taken from the high resolution transmission electron microscopy (HRTEM), of the acicular α-Ti and the β'-Ti. The *d*-spacing of the plane $(01\bar{1}0)$ for α-Ti was equal to 0.50 nm, while that of the $(3\bar{1}2)$ plane for β'-Ti was equal to 0.28 nm. The high resolution image, as shown in Fig. 4.6(e), of the marked area in Fig. 4.6(d) was simulated by a computer program (Digital Micrograph 3.3, Gatan Inc., Pleasanton, CA). It indicated that the ledge mechanism (labeled as "L") was probably the favorable precipitation mechanism of α-Ti from the matrix of β'-Ti. The ledge mechanism was frequently encountered in the partially coherent

interface consisting of many sets of edge dislocations or misfit dislocations. When the crystal structures of the matrix and the precipitate were different to a significant degree, the interface boundaries had to migrate by the ledge mechanism.[11] The ledge mechanism was reported, for instance, to be the growth mechanism of α and β interface boundaries in Ti-base alloy.[12] It was likely that the acicular α-Ti was also precipitated from β'-Ti matrix by means of the ledge mechanism.

Figure 4.7 shows the backscattered electron image of the reaction layers "E" and "F" together with "D" between Ti and ZrO_2 after reaction at 1550°C/6 h. The arrows in the upper middle indicated the original interface of Ti and ZrO_2. Abutting the zirconia side, the precipitate-free reaction layer "E" (gray), which dissolved a large amount of zirconium and oxygen, was β'-Ti in solid solution, consisting of 35.33 at.% Ti, 25.85 at.% Zr, and 38.82 at.% O measured by the EPMA. The formation of β'-Ti in solid solution, designated as β'-Ti(Zr, O), can be expressed as follows:

$$ZrO_2 + Ti \xrightarrow{\text{heating}} ZrO_{2-x} + \beta\text{-}Ti(Zr, O) \quad (3)$$

$$\beta\text{-}Ti(Zr, O) \xrightarrow{\text{cooling}} \beta'\text{-}Ti(Zr, O) \quad (8)$$

In contrast, β'-Ti (gray) and *c*-ZrO_{2-x} (bright, either rounded or Chinese-script-like) coexisted in the reaction layer "F." By the EPMA analyses, this β'-Ti contained 46.72 at.% Ti, 27.00 at.% Zr and 26.28 at.% O, meanwhile the Chinese-script-like *c*-ZrO_{2-x} contained 2.36 at.% Ti, 20.92 at.% Zr, 66.87 at.% O, 9.84 at% Y, displaying a large amount of yttrium, an effective stabilizer of *c*-ZrO_{2-x}. This is the reason why the zirconia was cubic symmetric in crystal structure. A few small rounded *c*-ZrO_{2-x} grains

were scattered near the interface, since *c*-ZrO_{2-x} grains were extensively dissolved into titanium. On the right-hand side of Fig. 4.7, Chinese-script-like *c*-zirconia phase (resembling the stroke of a calligraphic brush) was surrounded by the β'-Ti. The reason why *c*-ZrO_{2-x} became Chinese-script-like was still unclear at this moment. It was believed that zirconium was excluded from the metastable oxygen deficient zircronia during cooling. However, no α-Zr was found in the reaction layer "F" like in the reaction layer "G," since zirconium went into solid solution in β'-Ti (O, Zr). The formation mechanisms in the reaction layer "F" can be expressed as the following reactions:

$$ZrO_2 + Ti \xrightarrow{\text{heating}} ZrO_{2-x} + \beta\text{-}Ti(Zr, O) \quad (3)$$

$$ZrO_{2-x} \xrightarrow{\text{cooling}} \alpha\text{-}Zr + c\text{-}ZrO_{2-y\,(y<x)} \quad (9)$$

$$\alpha\text{-}Zr + c\text{-}ZrO_{2-y\,(y<x)} + \beta\text{-}Ti(Zr, O) \xrightarrow{\text{cooling}} c\text{-}ZrO_{2-y\,(y<x)} + \beta'\text{-}Ti(Zr, O) \quad (10)$$

Figure 4.8 displays the backscattered electron image and various characteristic x-ray maps of the reaction layers "F" after reaction at 1550°C/6 h. The x-ray mapping of Y in Fig. 4.8(b) indicated yttrium was hardly dissolved into titanium and then remained in both small spherical and Chinese-script-like zirconia. This is consistent with the results reported by Zhu *et al.,*[3] who found that yttrium element congregated and remained at the interface to form a high Y_2O_3 content of ZrO_2, when ZrO_2 reacted with molten titanium. The distributions of Ti, Zr, and O elements in the reaction layer "F" [Fig. 4.8 (c)-(e)] indicated that a significant amount of titanium diffused into to the ceramic side and reacted with zirconia to form β'-Ti(Zr,

O).

Figure 4.9(a) displays the backscattered electron image of the reaction layer "G" in the zirconia side far away from the interface after reaction at 1550°C/6 h. The distributions of Y, Ti, Zr, and O elements in the interface were demonstrated by individual characteristic x-ray mappings in Fig. 4.9(b)-(e), respectively. It indicated that a significant amount of oxygen was dissolved in α-Zr (bright), with both yttrium and titanium being scarcely dissolved into α-Zr. From the EMPA analyses, the α-Zr in the reaction layer "G" contained 1.05 at.% Ti, 57.5 4at.% Zr, 40.73 at.% O, and 0.68 at.% Y corresponding with α-Zr (O). Because the solubility of α-Zr in *c*- or *t*-ZrO_{2-x} declined as the temperature was lowered, as shown in the Zr-O phase diagram,[13] the α-Zr was segregated on grain boundaries during cooling by the exsolution of zirconium from ZrO_{2-x}, causing the increase in the O/Zr ratio of oxygen deficient zirconia.

The *c*-ZrO_{2-x} and the lenticular *t*-ZrO_{2-x} were observed in the gray region [Fig. 4.9(a)]. It was believed that the specimen was cooled down from the two-phase (*c* + *t*) region in the ZrO_2-Y_2O_3 phase diagram. The fact that the lenticular *t*-ZrO_2 with three variants was transformed in the *c*-ZrO_{2-x} had been reported by several previous studies.[6, 14-17] Lin and Lin[6] further found that the lenticular *t*-ZrO_{2-x} was formed in an ordered *c*-ZrO_{2-x},. It was worth noting that zirconia grains with a concentrated yttrium [Fig. 4.9(b)] had the cubic symmetry in crystal structure. The formation mechanisms in the reaction layer "G" can be expressed as the following reactions:

$$ZrO_2 + Ti \xrightarrow{\text{heating}} ZrO_{2-x} + \beta\text{-}Ti(O) \quad (1)$$

$$ZrO_{2-x} \xrightarrow{\text{cooling}} \alpha\text{-}Zr(O) + c\text{-}ZrO_{2-y\,(y<x)} + t\text{-}ZrO_{2-y\,(y<x)} \quad (11)$$

Based upon the foregoing results and discussion, the individual phases and formation mechanisms of the distinct reaction layers in the reaction affected zone between titanium and zirconia were summarized in Table 4.1.

4.3.2 Proposed Model of Microstructural Evolution

Even though extensive studies were carried out on the interface reaction between the titanium and zircronia, the microstructure evolution has not been elucidated to date. The information with regard to the relationships between the ternary constitution and the microstructures produced by isothermal diffusion among three elements is very sparse.[18] In the present study, the microstructure resulting from isothermal diffusion among titanium and zirconia is attempted to be inferred by the help of the Ti-Zr-O ternary phase diagram. However, only the isothermal Ti-Zr-O ternary phase diagram at 1450°C (not 1550°C) has been found in literature.[19] Assuming that the composition of the solid phases is approximated as constant between 1450° and 1550°C, the interpretation of the microstructure at the interface between Ti and ZrO_2 in term of the Ti-Zr-O phase diagram can be reasonably determined. The Ti-Zr-O phase diagram and the diffusion couple are somewhat different chemically. The ZrO_2 contains 3 mol% Y_2O_3, so it is out of the Ti-Zr-O ternary system. However, this probably does not have much effect on the results and the effect can be negligible in this study.

Figure 4.10 shows the microstructural evolution at the interface between titanium and zirconia diffusion couple after annealing at 1550^{o}C based upon the observation and analyses mentioned above. Figure 4.10 (a) illustrates the titanium and zirconia diffusion couple prior to the anneal heat treatment, indicating the original interface and finely distributed ZrO_2 grains. When

titanium was held in contact with zirconia at high temperatures, diffusion layers would develop.

By cross-examining the experimental results and the ternary phase diagram, it was proposed that all gross compositions, in various vertical slices along the longitudinal direction perpendicular to the interface, lay upon the line *a-b-c-d-e,* or the so called diffusion path, in the Ti-Zr-O ternary system at 1450ºC.[19] As shown in Fig. 4.10(b), the diffusion path crosses the fields of β-Ti, α-Ti + β-Ti, β-Ti, β-Ti + *t*-ZrO_2, α-Zr + β-Ti + *t*-ZrO_2, and α-Zr + *t*-ZrO_2.

It is well known that the divariant or three-phase regions in the ternary phase diagram simply are in correspondence to the interfaces between layers in the diffusion couple which is isothermally annealed at high temperatures. Conversely, ternary isothermal diffusion can result in the formation of both one-phase and two-phase layers in the diffusion couple, but not three-phase layers.[18] As a result, in the Ti-ZrO_2 diffusion couple, the layers of β-Ti, α-Ti + β-Ti, β-Ti, β-Ti + *t*-ZrO_2, and α-Zr + *t*-ZrO_2 would have been observed in sequence from Ti to ZrO_2, but not the layers of α-Zr + β-Ti + *t*-ZrO_2 at all. The region of α-Zr + β-Ti + *t*-ZrO_2 in the Ti-Zr-O ternary phase diagram was represented in the diffusion couple by the interface between the layers of β-Ti + *c*-ZrO_2 and α-Zr + *c*-ZrO_2 as shown in Fig. 4.10(c). Furthermore, as illustrated in Fig. 4.10(b) the β-Ti layer, corresponding to the layer "A," varied in composition from Ti to β_a. The α in the α-Ti + β-Ti layer should vary from α_a to α_b and the β from β_a to β_b, while the β-Ti, corresponding to the layers "D" and "E", varied from β_b to β_c.

In the case of Ti-ZrO_2 diffusion couple where the reaction was predominant in the initial stage and the diffusion velocities of the three components were

markedly different, the diffusion path deviated from the direct path between the compositions of the end points, i.e., Ti and ZrO_2 in the present study. It was believed that the oxidation – reduction reaction in the initial stage shifted the end point in the ceramic side to the two-phase region of α-Zr + *t*-ZrO_2, presumably to point *e*. Besides, it was unlikely that the diffusion path went through the region of α-Ti + β-Ti + *t*-ZrO_2 since it was impossible for such an interface to exist in between the layers of α-Ti + β-Ti and β-Ti + *t*-ZrO_2. It was also noted that the layer of α-Zr + β-Ti was not observed in the present study. As a consequence, the ternary diffusion path *a-b-c-d-e* provided the best approximation that could be made at present.

In reality, the high chemical affinity of titanium to oxygen caused the formation of oxygen-dificient zirconia (ZrO_{2-x}), indicating that the oxidation – reduction reaction predominated in the initial stage before the diffusion prevailed. A significant increase in oxygen vacancies, as a consequence of the oxidation – reduction reaction between titanium and zirconia, triggered the stabilization effect of zirconia. The zirconia in the Ti-Zr-O ternary phase diagram, shown in Fig. 4.10(b), would be in the cubic phase instead of tetragonal phase when the Ti/ZrO_2 diffusion couple was isothermally annealed at 1550^{o}C.[6]

The various layers formed during cooling stage are displayed in Figure 4.10(d). The β-Ti layer abutting the reaction-unaffected Ti, with a small amount of Zr in solid solution, was transformed to α-Ti (designated as layer "A") on cooling, and the continuous lamellar Ti_2ZrO + α-Ti (designated as layer "B") is attributed to the precipitation of Ti_2ZrO in the metastably transformed α-Ti matrix. Ti_2ZrO was precipitated from α-Ti in the α-Ti + β-Ti layer during cooling, leading to the existence of the lamellar (Ti_2ZrO + α-Ti) + β'-Ti region (designated as layer "C"). In the layer "D," the β-Ti

was transformed to β'-Ti where the acicular α-Ti was precipitated, meanwhile a continuous β'-Ti(Zr, O) with a large amount of Zr in solid solution was found near the interface (designated as layer "E"). In the zirconia side, the dissolution of titanium in zirconia led to the formation of β-Ti(Zr, O) and suppressed grain growth of zirconia near the interface. During cooling, β'-Ti(Zr, O) and cubic ZrO_{2-x}, with high yttrium, were formed in the reaction layer "F." Because of very low solubility in titanium, almost all of yttrium remained in zirconia, resulting in the stabilization of *c*-ZrO_{2-x} during cooling down to room temperature. Away from the original metal-ceramic interface, ZrO_2 was dramatically reduced to ZrO_{2-x} by titanium, accompanied by a significant grain growth of ZrO_{2-x} on heating. The intergranular α-Zr was excluded from the metastable oxygen deficient zirconia, while the lenticular *t*-ZrO_2 and ordered *c*-ZrO_{2-x} were formed from the *c*-ZrO_{2-x} matrix during cooling (the reaction layer "G").

4.4 Conclusions

1. The diffusional reaction between titanium and zirconia was carried out at 1550°C in argon. In the metal side, there existed five reaction layers in a sequence of α-Ti(O), Ti_2ZrO + α-Ti(O, Zr), Ti_2ZrO + α-Ti(O, Zr) + β'-Ti (O, Zr), α-Ti (O, Zr) + β'-Ti (O, Zr), and β'-Ti (Zr, O) after cooling.
2. In the zirconia side, two reaction layers were found: near the original interface, β'-Ti coexisted with fine spherical *c*-ZrO_{2-x} and Chinese-script-like *c*-ZrO_{2-x}; further away from the original interface, the coarsened intergranular α-Zr, lenticular *t*-ZrO_{2-x} and ordered *c*-ZrO_{2-x} were found.
3. The acicular α-Ti and the β'-Ti showed two different orientation relations. One of the orientation relations was determined to be $[2\bar{1}\bar{1}0]_{\alpha\text{-Ti}}$ // $[001]_{\beta'\text{-Ti}}$ and $(0001)_{\alpha\text{-Ti}}$ // $(100)_{\beta'\text{-Ti}}$ and the other was $[2\bar{1}\bar{1}0]_{\alpha\text{-Ti}}$ //

$[021]_{\beta'\text{-Ti}}$ and $(0001)_{\alpha\text{-Ti}}$ // $(1\bar{1}2)_{\beta'\text{-Ti}}$.

4. Based upon the experimental results in this study, the diffusion path, connecting phases formed by the reaction between Ti and ZrO_2, was drawn on the Ti-Zr-O ternary phase diagram.
5. The information with regard to the relationships between the Ti-Zr-O ternary phase diagram and the microstructures produced by isothermal diffusion between Ti and ZrO_2 at 1550°C has been provided.

Acknowledgment

The authors would like to thank the National Science Council of Taiwan for financially supporting this research under Contract No. NSC 92-2216-E-009-027. We also pay our appreciation to Mr. Chi-Ming Wen in Chung-Shan Institute of Science and Technology for preparing the hot-pressed specimens.

References:

1. B. C. Weber, H. J. Garrett, F. A. Mauer, and M. A. Schwartz, "Observations on the Stabilization of Zirconia," *J. Am. Ceram. Soc.*, **39**[6]**,** 197-07 (1956).
2. R. Ruh, N. M. Tallan, and H. A. Lipsitt, "Effect of Metal Additions on the Microstructure of Zirconia," *J. Am. Ceram. Soc.*, **47**[12]**,** 632-35 (1964).
3. J. Zhu , A. Kamiya, T. Yamada, W. Shi, K. Naganuma, and K. Mukai, "Surface tension, Wettability and Reactivity of Molten Titanium in Ti/Yttria-Stabilized ZirconiaSystem," *Mater. Sci. Engng. A*, **A327**,117-27 (2002).
4. K. F. Lin and C. C. Lin, "Transmission Electron Microscope Investigation of The Interface between Titanium and Zirconia," *J. Am. Ceram. Soc.*, **82**[11]**,** 3179-85 (1999).

5. K. L. Lin and C. C. Lin, "Ti_2ZrO Phases Formed in the Titanium and Zirconia Interface after Reaction at 1550°C," *J. Am. Ceram. Soc.,* **88**[5], 1268-272 (2005).
6. K. L. Lin and C. C. Lin, "Zirconia-Related Phases in the Zirconia/Titanium Diffusion Couple after Annealing at 1100° to 1550°C," accepted by *J. Am. Ceram. Soc.,* (2005).
7. G. Cliff and G. W. Lorimer, "The Quantitative Analysis of Thin Spectimens, " *J. Microsc.,* **130** [3], 203-07 (1975).
8. J. I. Goldstein, *Scanning Electron Microscopy and X-ray Microanalysis, 2nd ed.,* Plenum Press, New York, 1992.
9. J. L. Murray and H. A. Wriedt, "The Titanium-Zirconium System"; pp. 340-45 in Phase *Diagrams of Binary Titanium Alloys. Edi*ted by J. L. Murray. ASM International, Metals Park, OH, 1987.
10. G. Lutjering and J. C. Williams, *Titanium; Ch*. 5, p. 177, Springer-Verlag, Berlin, Germany,. 2003.
11. D. A. Porter and K. E. Easterling, "Phase Transformations in Metals and Alloys" Chapman Hall, New York, 1992.
12. T. Furuhara, H. J. Lee, E. S. K. Menon, and H. I. Aaronson, "Interphase Boundary Structures Associated with Diffusional Phase Transformations in Ti-Base Alloys," *Metall. Trans. A,* **21A**,1627-43 (1990).
13. H. Baker, *ASM Handbook, Vo*l. 3, Alloy *Phase Diagrams; p.* 2326. ASM International, Metals Park, OH, 1992.
14. A. H. Heuer and M. Rühle, "Phase Transformations in ZrO_2-Containing Ceramic: I, The Instability of c-ZrO_2 and the Resulting Diffusion-Controlled Reactions"; pp. 1-13 in *Advances in Ceramics, Vol. 12, Science and Technology of Zirconia II. Edi*ted by N. Claussen, M. Rühle and A. H. Heuer. American Ceramic Society, Columbus, OH, 1984.

15. V. Lanteri, A. H. Heuer, and T. E. Mitchell, "Tetragonal Phase in the System ZrO_2- Y_2O_3"; pp.118-30 in Adva*nces in Ceramics, Vol. 12, Science and Technology of Zirconia II. Edi*ted by N. Claussen, M. Rühle and A. H. Heuer. American Ceramic Society, Columbus, OH, 1984.
16. R. Chaim, M. Rühle, and A. H. Heuer, "Microstructural Evolution in a ZrO_2-12 Wt% Y_2O_3 Ceramic," *J. Am. Ceram. Soc.,* **68**[8]**,** 27-31 (1985).
17. A. H. Heuer, V. Lanteri, and A. Dominguez-Rodriguez, "High-Temperature Precipitation Hardening of Y_2O_3 Partially-Stabilized ZrO_2 (Y-PSZ) Single Crystals," *Acta metall.,* **37**[2]**,** 559-67 (1989).
18. F. N. Rhines, “Phase Diagrams in Metallurgy: Their Development and Application,” pp. 156-157, McGraw-Hill Book Company, 1965.
19. “Phase Diagrams for Zirconium + Zirconia Systems,” ed. By H. M. Ondik and H. F. McMurdie, p.12, The American Ceramic Society, OH, 1998.

Table 4.1 Microstructural features and formation mechanisms of various phases at the interface of Ti and ZrO_2 at 1550°C

Ti/ZrO_2 Diffusion Couple	Reaction Layer	Phases	Formation Mechanisms
Metal Side	"A"	α-Ti(O)	Equation (1) and (2)
	"B"	α-Ti(Zr, O) Ti_2ZrO	Equation (3) and (4)
	"C"	α-Ti(Zr, O) Ti_2ZrO β'-Ti(Zr, O)	Equation (5) and (6)
	"D"	α-Ti(Zr, O) β'-Ti	Equation (3) and (7)
	"E"	β'-Ti(Zr, O)	Equation (3) and (8)
Zirconia Side	"F"	β'-Ti(Zr, O) c-ZrO_{2-x}	Equation (3), (9), and (10)
	"G"	α-Zr(O) t-ZrO_{2-x} c-ZrO_{2-x}	Equation (1) and (11)

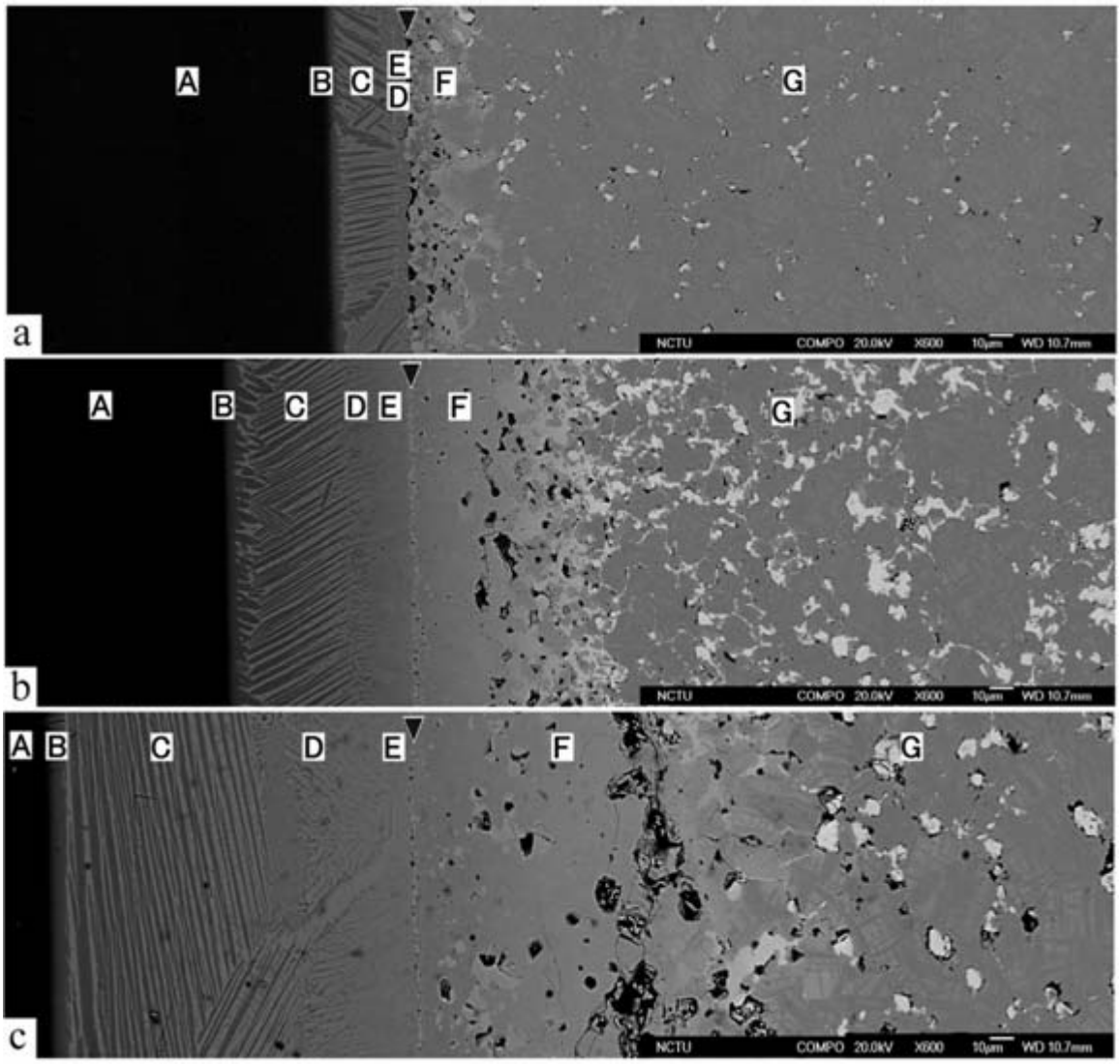

Fig. 4.1 (a), (b), and (c) SEM micrographs (backscattered electron image, BEI) of the cross-sectional between Ti/ZrO_2 after reaction at 1550°C/0.5 h, 3h, and 6h, respectively. The arrows indicated the interface between Ti/ZrO_2.

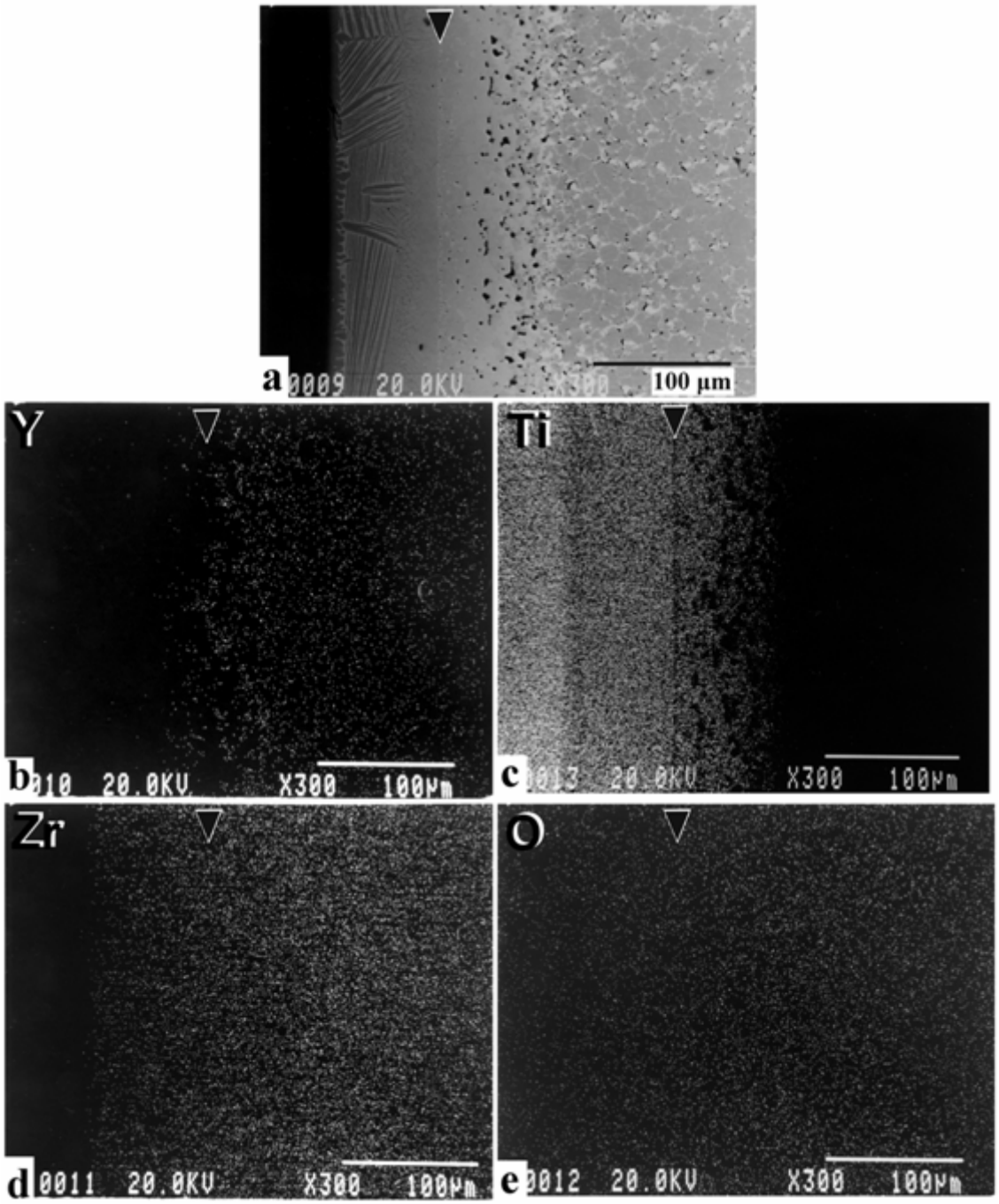

Fig. 4.2 (a) SEM micrograph (backscattered electron image, BEI) of the cross-sectional between Ti/ZrO_2 after reaction at 1550^{o}C/6 h; (b)~(e) X-ray maps of Y, Ti, Zr, and O, respectively.

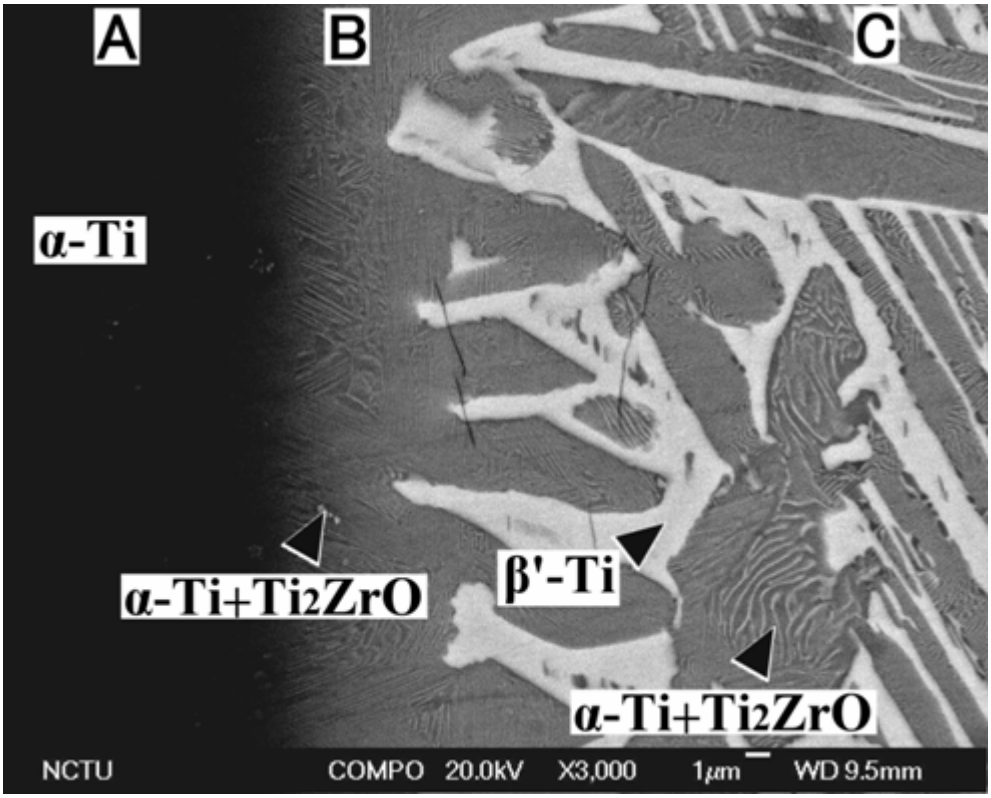

Fig. 4.3 SEM micrograph (backscattered electron image, BEI) of the reaction layers "A", "B", and "C" in the interface between Ti/ZrO_2 after reaction at $1550^oC/6$ h.

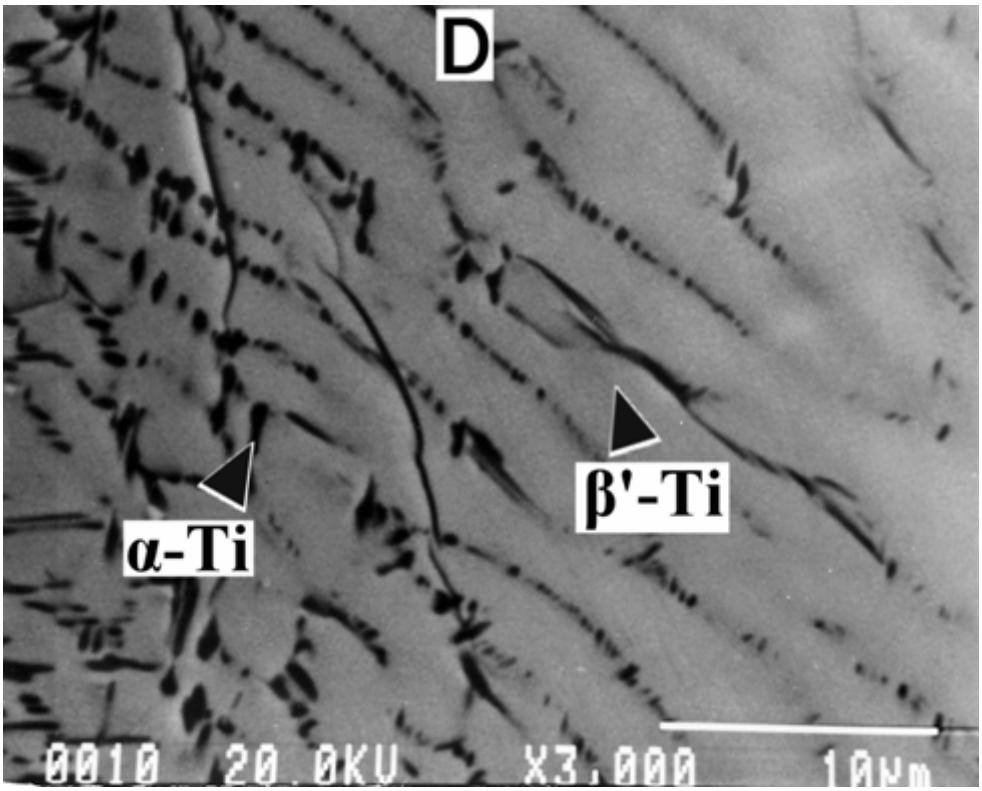

Fig. 4.4 SEM micrograph (backscattered electron image, BEI) of the reaction layer "D" in the interface between Ti/ZrO_2 after reaction at 1550^{o}C/6 h.

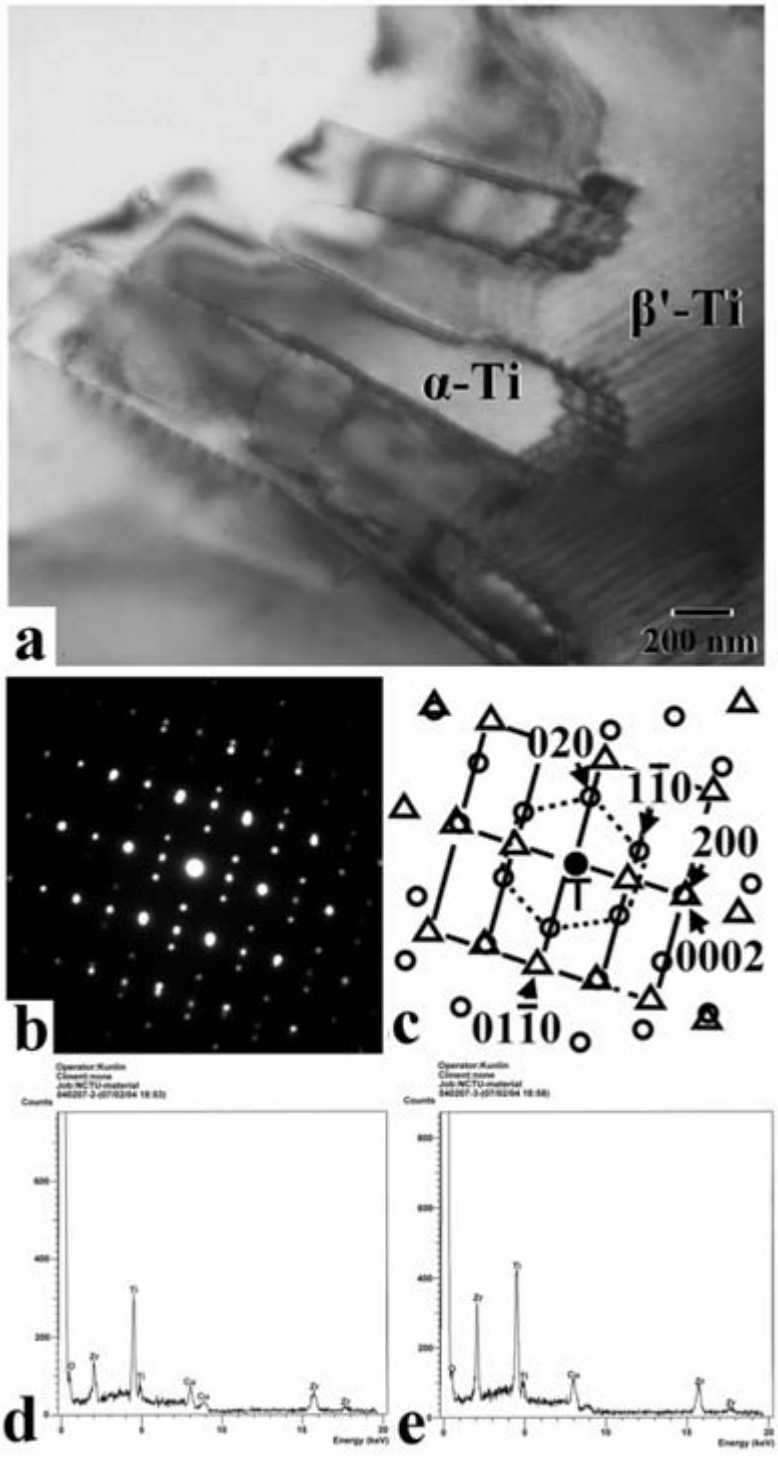

Fig. 4.5 (a) TEM micrograph (bright field image, BFI) of the cross-sectional between Ti/ZrO_2 after reaction at 1550^{o}C/6 h; (b) and (c) selected area diffraction patterns of the α-Ti and β'-Ti, $Z=[2\bar{1}\bar{1}0]_{\alpha\text{-Ti}}$ //$[001]_{\beta'\text{-Ti}}$ and its schematic diagram (Δ: α-Ti, ○: β'-Ti), respectively; (d) and (e) energy-dispersive spectra of α-Ti and β'-Ti.

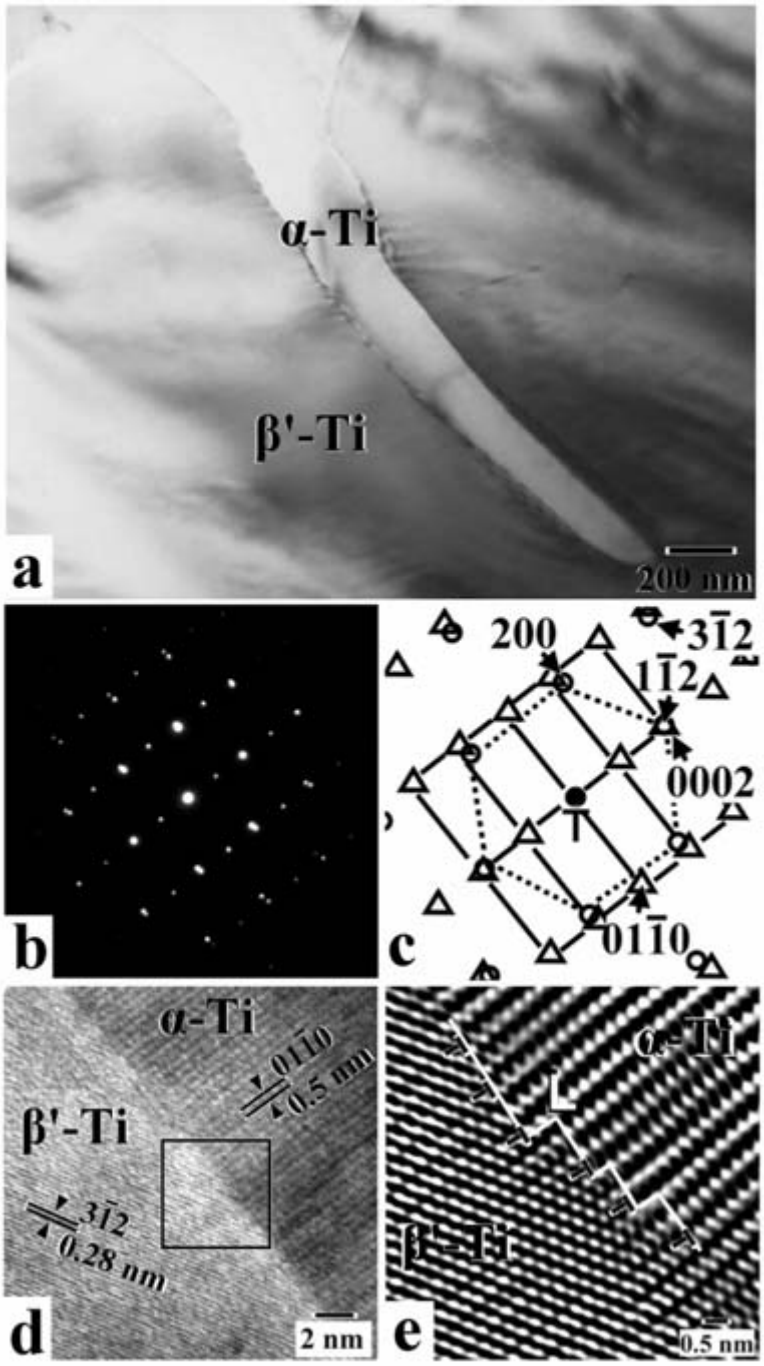

Fig. 4.6 (a)TEM micrograph (bright field image, BFI) of the cross-sectional between Ti/ZrO_2 after reaction at 1550^{o}C/6 h; (b) and (c) selected area diffraction patterns of the α-Ti and β'-Ti, $Z=[2\ \bar{1}\ \bar{1}\ 0]_{\alpha\text{-Ti}}$ // $[021]_{\beta'\text{-Ti}}$ and its schematic diagram (Δ: α-Ti, ○: β'-Ti), respectively; (d) images taken form the high resolution transmission electron microscopy (HRTEM) of acicular α-Ti and β'-Ti; (e) the computer simulation in the marked area of Fig. 4.3(d).

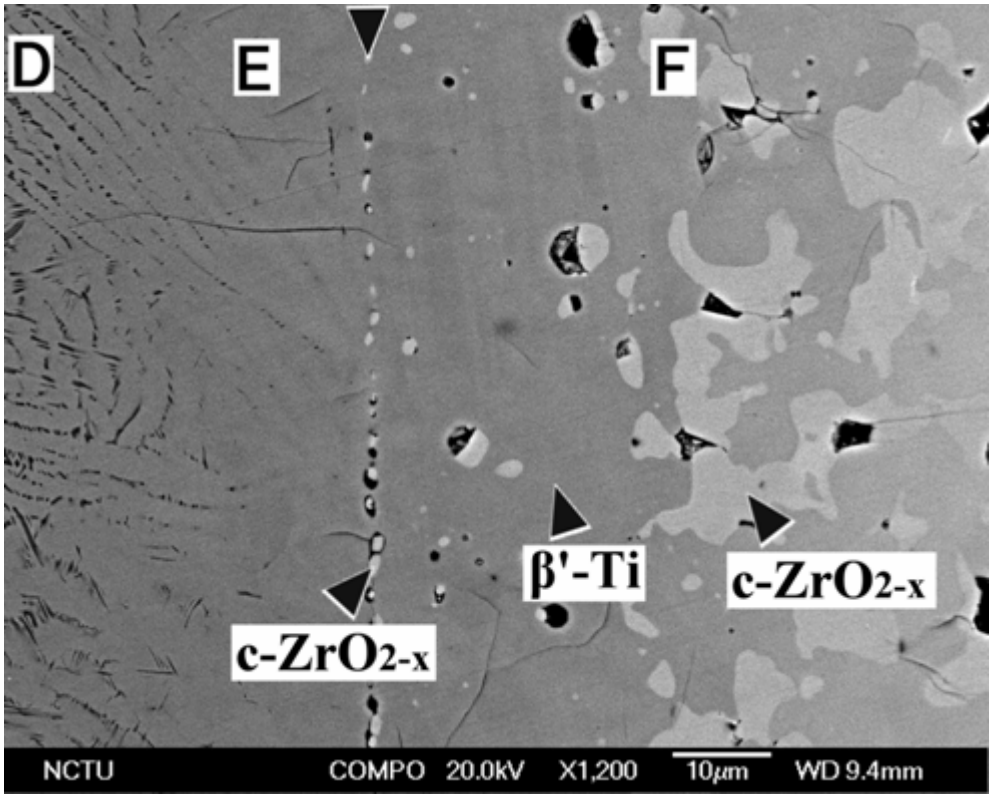

Fig. 4.7 SEM micrograph (backscattered electron image, BEI) of the reaction layers "D", "E", and "F" in the interface between Ti/ZrO_2 after reaction at 1550°C/6 h.

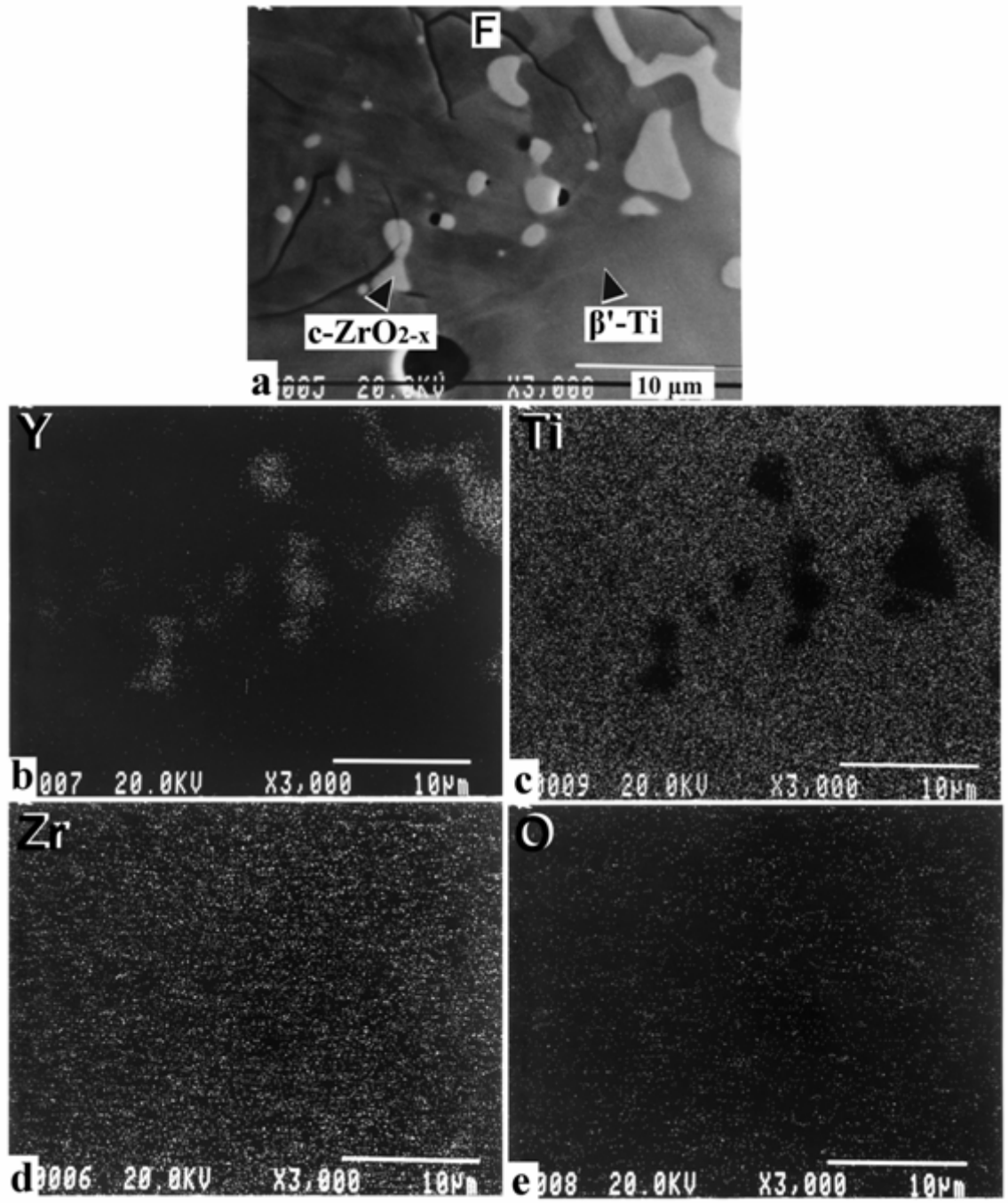

Fig. 4.8 (a) SEM micrograph (backscattered electron image, BEI) of the reaction layers "F" in the interface between Ti/ZrO_2 after reaction at 1550^{o}C/6 h ; (b)~(e) X-ray maps of Y, Ti, Zr, and O, respectively.

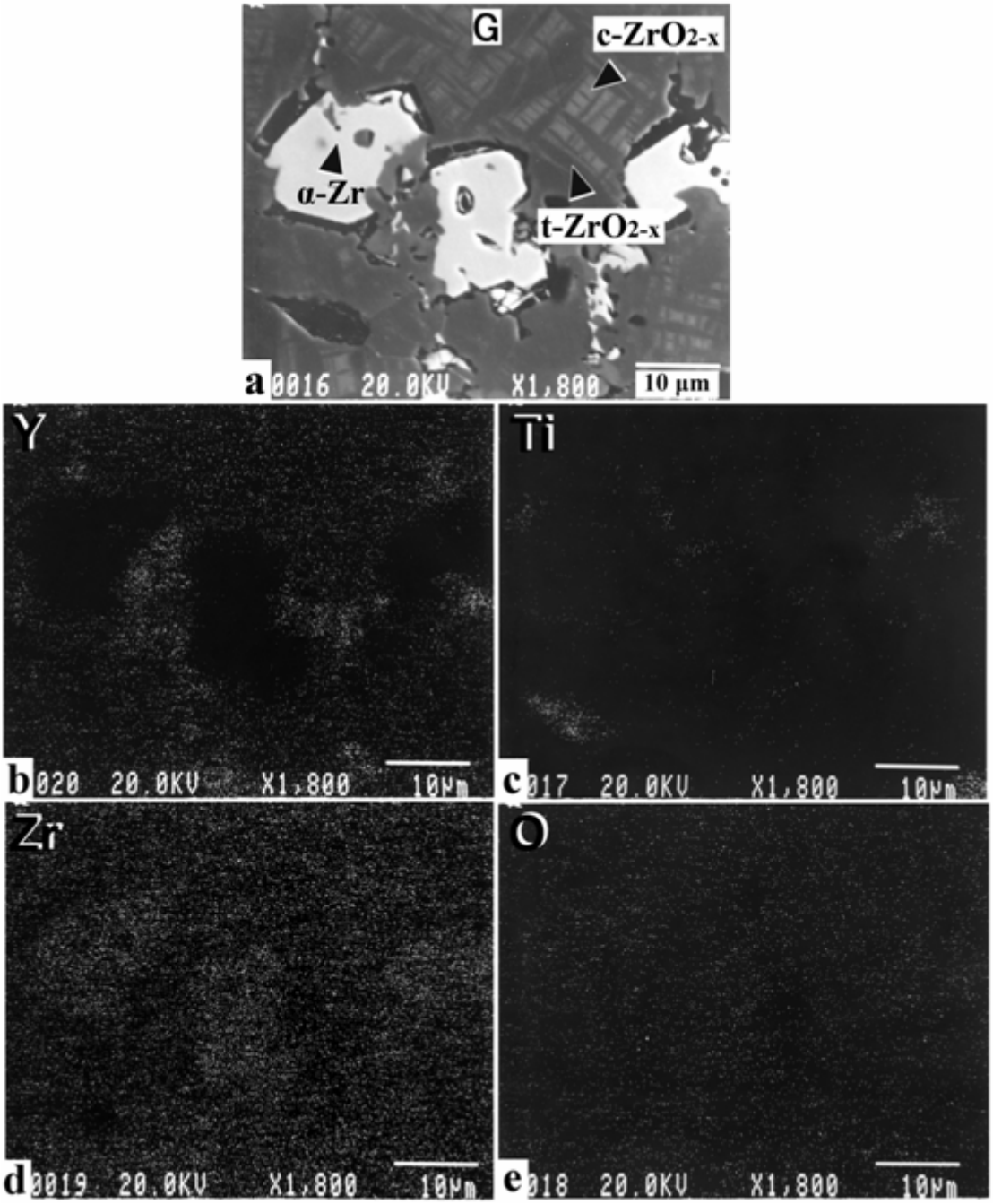

Fig. 4.9 (a) SEM micrograph (backscattered electron image, BEI) of the reaction layer "G" in the zirconia side away from the interface after reaction at 1550^{o}C/6 h; (b)~(e) X-ray maps of Y, Ti, Zr, and O, respectively.

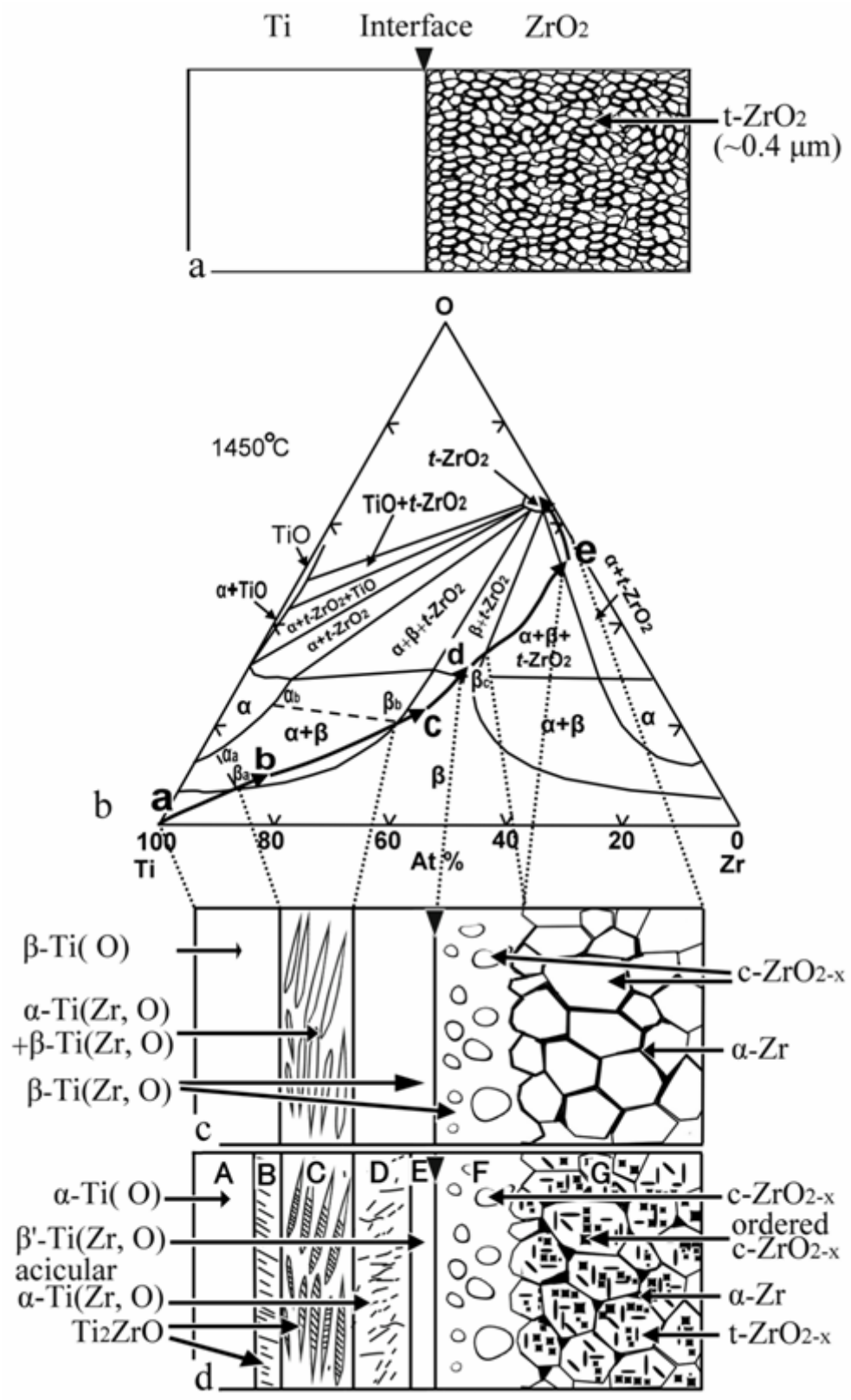

Fig. 4.10 Schematic diagrams showing the microstructural evolution of the Ti/ZrO_2 diffusion couple annealed at 1550°C. (a) as hot-pressed; (b) the Ti-Zr-O ternary system at 1450ºC[19]; (c) the structure of the Ti/ZrO_2 diffusion couple annealed at 1550ºC, and (d) the structure on cooling.